Interlayer exchange coupling in epitaxial Fe/Cr/Fe/Ag/GaAs(100) structures

R. J. Hicken, C. Daboo, M. Gester,[a] A. J. R. Ives, S. J. Gray, and J. A. C. Bland
The Cavendish Laboratory, University of Cambridge, Madingley Road, Cambridge CB3 0HE, United Kingdom

(Received 9 June 1995; accepted for publication 10 August 1995)

The interlayer exchange coupling has been investigated in epitaxial Fe(20 Å)/Cr/Fe(20 Å)/Ag/GaAs(100) structures that contain a wedge-shaped (0–40 Å) Cr layer. Longitudinal and polar magneto-optical Kerr-effect (MOKE) and Brillouin light-scattering measurements have been combined to determine values for the relevant anisotropy constants and both the bilinear and biquadratic coupling strengths. The phase and period of the oscillations in the interlayer coupling are found to agree well with those reported by other researchers while the total coupling strength is found to be reduced. This reduction is presumably due to the presence of structural imperfections in our samples, and our results may therefore be of use in testing some of the recently proposed extrinsic biquadratic coupling mechanisms. Specifically, we find that for the Cr thicknesses studied the biquadratic coupling strength in our samples varies as $d_{\mathrm{Cr}}^{-1.4}$ where d_{Cr} is the thickness of the Cr layer. We also present results that show how the ultrathin Cr limit may be investigated. We show that the coercivity of the easy axis MOKE loops is sensitive to submonolayer coverages of Cr and that polar MOKE is sensitive to the strong ferromagnetic coupling found in the 0–4 Å Cr thickness range. © *1995 American Institute of Physics.*

I. INTRODUCTION

Antiferromagnetic (AFM) interlayer exchange coupling through a transition-metal spacer layer was first observed in Fe/Cr/Fe trilayer structures.[1] The subsequent discovery of a giant magnetoresistance (GMR) effect[2] in Fe/Cr multilayers, which is of potential technological significance, has lead to great interest in this field and interlayer exchange coupling and GMR have subsequently been observed in a number of other multilayered materials.[3] The Fe/Cr system has, however, been particularly important in the development of our understanding of the interlayer coupling mechanism, since it was in the Fe/Cr system that it was first demonstrated that: the interlayer coupling energy is of the Heisenberg or bilinear form, being proportional to the scalar product of the layer magnetizations;[4] the sign of the interlayer coupling oscillates as a function of the spacer thickness;[5] the bilinear energy term may be augmented by a higher-order term, the so called biquadratic coupling term.[6] In fact Cr is a particularly interesting choice of spacer material because bulk Cr is known to exhibit incommensurate spin density wave antiferromagnetism.[7] Structures grown on Fe(100) whiskers are believed to have the flattest interfaces that can be currently obtained and it was in such structures that the interlayer coupling was first observed to oscillate with a period of approximately two atomic monolayers.[8,9] It was subsequently demonstrated that these short period coupling oscillations are correlated with the AFM ordering of the Cr.[10] While attempts are being made to unite the various theories of interlayer coupling,[11] there is general agreement that the period of the coupling oscillations is determined by the geometry of the Fermi surface of the spacer material, which also determines the AFM ordering of the Cr. It is somewhat surprising then that Cr spacer layers of different orientations should yield identical coupling periods.[12] We should consider also that the magnetic structure of thin films of Cr may be different to that of bulk Cr and indeed an enhanced Néel temperature has already been observed[10] in the former. Recent studies using Fe whisker substrates[13,14] have provided information concerning the phase of the short period coupling oscillations. One surprising result was that AFM coupling was obtained after 5 monolayers of Cr growth. A possible explanation may be that the first 2 monolayers of Cr have ferromagnetic (FM) rather than AFM alignment.[15] Clearly trilayers containing Cr layers of a few monolayers thickness are of considerable interest but it is expected that roughness and pinhole coupling will affect both the strength of the coupling and the magnetic ordering of the Cr.[16]

The biquadratic coupling strength in Fe/Cr/Fe structures has been observed to be of similar magnitude to the bilinear coupling strength[14,17] and a number of mechanisms has been proposed to explain the origin of the biquadratic coupling. Those that apply to ideal structures with flat interfaces,[18–22] the so-called intrinsic mechanisms, are found to predict only very small values for the biquadratic coupling strength. The so-called extrinsic mechanisms take into account the effects of roughened interfaces,[23,24] loose spins in the spacer material,[25] and pinholes through the spacer layer.[26,27] Researchers have examined the temperature dependence of the biquadratic coupling in order to differentiate between the mechanisms listed above (see Ref. 25 and the references therein) and on this basis for Fe/Cr structures grown on Fe whiskers it was concluded that there must be a strong contribution from an intrinsic mechanism.[28] In order to explore the relevance of the various proposed extrinsic mechanisms there is clearly a need for studies of relatively structurally imperfect samples in which both coupling constants are accurately determined.

[a]Present address: I.P.C.M.S., Bâtiment 69, 23 rue du Loess, 67037 Strasbourg, France.

 0021-8979/95/78(11)/6670/9/$6.00

In this work we present a study of the interlayer coupling in Fe/Cr/Fe trilayer structures, containing wedge-shaped Cr layers, grown on Ag/GaAs(100) substrates. We have combined in-plane magneto-optical Kerr-effect (MOKE), polar MOKE, and Brillouin light-scattering (BLS) measurements in order to investigate how the bilinear and biquadratic coupling strengths depend upon the value of the Cr thickness. Although short period coupling oscillations can be obtained for such structures grown at elevated temperatures,[29] our samples were grown at lower temperatures where rougher interfaces are expected to result. We discuss how our deduced values of the bilinear coupling strength compare with those of other researchers and present our results for the Cr thickness dependence of the biquadratic coupling strength. BLS and polar MOKE are sensitive to the perpendicular anisotropy of the constituent Fe layers and interlayer coupling of either sign. We discuss how this allows us to characterise the magnetic behavior for Cr thicknesses in the monolayer regime and we show how the coercivity of the easy axis MOKE loop changes in this same region.

II. SAMPLE GROWTH

The Fe/Cr/Fe structures described in this article were grown on Si-doped GaAs(100) substrates capped with thick Ag(100) buffer layers. While direct growth on to an insulating substrate would be preferable for transport measurements, it is well known that the chemistry of the Fe/GaAs interface is complicated by interdiffusion.[30] The Ag buffer layer therefore provides a flat substrate that will not interdiffuse with the deposited film. The surface of the GaAs substrate initially has an oxidized surface layer that is removed by annealing at a temperature of 620 °C for 30 min.[31] Cycles of sputtering and annealing at 600 °C are then employed to remove any carbon present and to smooth the surface. The observation of a $p(4\times6)$ reconstruction by low-energy electron diffraction (LEED) then indicates that the surface is periodic over distances in excess of 100 Å. Reflection high-energy electron diffraction has also been used to confirm the flatness of the GaAs at this point.[32] Next it is necessary to grow an Fe seed layer in order to force the following Ag layer into the (100) orientation.[33] An Fe layer of thickness 15 Å is grown at a substrate temperature of 150 °C before the Ag layer of approximately 1000 Å thickness is grown at ambient temperature at a rate of about 5 Å per minute. The Ag layer is annealed at 300 °C for 1 h so that sharp LEED spots are obtained. The ⟨011⟩ axes of the Ag(100) layer lie parallel to the ⟨001⟩ axes of the Fe(100) seed layer. We should point out that the Fe seed layer is at best weakly ferromagnetic. The thick Ag buffer layer ensures that the Fe seed layer is not sensed by any of our magneto-optical measurements and so we do not discuss it further when considering the magnetic properties of the sample.

The trilayer structure is grown at ambient temperature. During the deposition of the first Fe layer LEED patterns taken between Bragg conditions show considerable spot broadening which indicates imperfect wetting of the Ag by the Fe. After deposition of the first 20 Å layer of Fe the sample is annealed at 150 °C for 30 min. Cross-shaped LEED spots then indicate the presence of steps parallel to the Fe⟨001⟩ axes, which are found to propagate through the rest of the structure. The Cr wedge layer is grown by moving the substrate behind a fixed shutter through a distance of 12 mm in steps of 0.2 mm. The completed structure is capped with about 20 Å of Cr that has been shown by electron-energy-loss spectroscopy[34] to be sufficient to prevent oxidation of the underlying Fe layers. The thicknesses of the various layers were obtained by monitoring the deposition rate with quartz crystal oscillators which were calibrated by profilometer measurements made on specially grown thicker films.

III. EXPERIMENTAL CONSIDERATION

In-plane MOKE measurements were made using an apparatus developed for vector magnetometry.[35] Hysteresis loops were recorded with the field applied parallel to both the in-plane easy, Fe⟨001⟩, and hard, Fe⟨011⟩, axes. The HeNe laser beam was focused to a spot of about 0.2 mm diameter and scanned along the wedge by moving the sample with a linear translation stage that is capable of a 1 μm positioning accuracy. Let us assume the interlayer coupling energy to be a surface energy of the form

$$E_{\text{coupling}} = -2A_{12}\hat{\mathbf{M}}_1\cdot\hat{\mathbf{M}}_2 - 2B_{12}(\hat{\mathbf{M}}_1\cdot\hat{\mathbf{M}}_2)^2, \tag{1}$$

in which $\mathbf{M}_1$ and $\mathbf{M}_2$ are the magnetization vectors of the two Fe layers and A_{12} and B_{12} are the bilinear and biquadratic coupling constants, respectively. By considering the condition for the saturated state to become unstable one finds an expression for the saturation field of the form

$$H_{\text{sat}} = \pm\frac{2K_1}{M} - \frac{4(A_{12}+2B_{12})}{Md}, \tag{2}$$

in which K_1, M, and d are the cubic anisotropy constant, magnetization, and thickness of the Fe layers (assumed to be equal), respectively. The positive and negative signs refer to the hard and easy axis directions, respectively. As we see later, Eq. (2) may be inapplicable when the demagnetization process occurs by domain-wall motion. These expressions also apply only when the coupling field is antiferromagnetic in nature, i.e., the second term in Eq. (2) is greater than zero. If the coupling field is ferromagnetic then we simply have $H_{\text{sat}} = \pm 2K_1/M$, where the negative case refers to the coercive field of a square easy axis hysteresis loop. Although the saturation field in Eq. (2) gives the total coupling strength the individual values of A_{12} and B_{12} can sometimes be deduced by considering other features in the hysteresis loop.[6,17] Since a hysteresis loop may be obtained within a matter of seconds and since theoretical loops are readily generated numerically[36] in-plane MOKE is a very convenient technique for the determination of interlayer coupling constants.

Polar MOKE measurements have been made inside a 7 T superconducting magnet in steps of about 0.1 mm along the length of the sample, as has been described previously.[37] Let us consider now a trilayer structure in which the two magnetic layers are identical apart from their interface anisotropies. Let us define the quantity

$$H_{a,i} = 4\pi M - \frac{2K_1}{M} - \frac{4K_{s,i}}{Md}, \tag{3}$$

in which $K_{s,i}$ is the interface anisotropy constant averaged over the two interfaces of layer i, where $i=1$ or 2. We may assume that close to saturation the magnetisation vectors and the surface normal are coplanar, and then we obtain the following expression for the saturation field:

$$A_{12}+2B_{12}=\frac{Md(H_{\rm sat}-H_{a,1})(H_{\rm sat}-H_{a,2})}{2(H_{a,1}+H_{a,2}-2H_{\rm sat})}, \tag{4}$$

which reduces to the simple form

$$H_{\rm sat}=H_a-\frac{4(A_{12}+2B_{12})}{Md} \tag{5}$$

for the case of antiferromagnetic coupling only when we assume that $H_{a,1}=H_{a,2}=H_a$. This was one of the approximations made in Ref. 37. However, we shall see that in fact for the samples to be described here $H_{a,1}\neq H_{a,2}$, and then Eq. (4) predicts that the polar MOKE saturation field has a nonlinear dependence upon the coupling field and is sensitive to both FM and AFM coupling.

The apparatus used to perform BLS measurements has been described previously.[38] The focused spot was scanned along the wedge by moving the sample with a translation stage capable of 0.1 mm positioning accuracy. The magnetic field was applied parallel to the short side of the sample, an Fe ⟨110⟩ direction, due to the limited pole piece separation of our magnet. In order to analyze our results, the theory that we used in Ref. 38 has been extended to include biquadratic coupling and to allow for the effect of the layer magnetizations canting away from the applied field direction. This canting behavior is most reliably calculated for the case that the field is applied along a hard axis direction as in our experimental arrangement. The full theory requires evaluation of large complex determinants, so we have also employed a simplified theory in which the dynamical magnetization is assumed to be independent of the coordinate that describes the position along the film normal.[39] This reduced theory is then essentially a uniform mode Ferromagnetic resonance (FMR) calculation but with additional effective fields included to describe the dipolar fields that result from the in-plane wave-vector component of the spin wave mode. The algebraic expressions that are obtained are sufficiently simple that they may be combined with standard optimisation routines to obtain a chi square fit to the BLS data. In this article all fits to the BLS data have been performed with the reduced theory although each of the best fits was recalculated with the full theory in order to investigate the magnitude of the error associated with the use of the reduced theory.

Since the wedge sample must be repositioned for the in-plane MOKE, polar MOKE, and BLS experiments we estimate that positions on the wedge correspond to within about 0.2 mm which implies a systematic error of up to 0.7 Å in the Cr thickness between the various experiments.

IV. RESULTS

We now describe in detail the results obtained for an Fe(20 Å)/Cr(0–38 Å)/Fe(20 Å) trilayer structure (sample I). In-plane easy and hard axis MOKE loops and polar MOKE loops were taken at various points along the wedge. Since

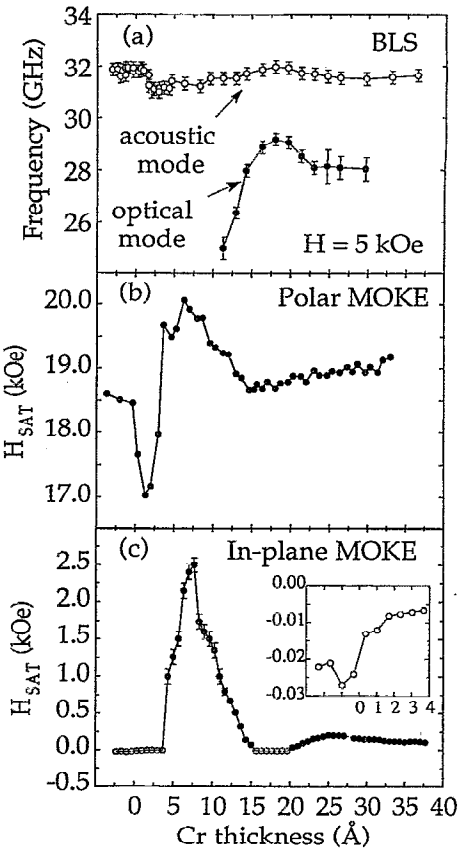

FIG. 1. The following quantities are plotted as a function of Cr thickness for sample I: (a) BLS mode frequencies, where the open and solid symbols denote the acoustic and optical modes, respectively; (b) the polar MOKE loop saturation field; (c) the in-plane easy axis MOKE saturation field (solid symbols), or the coercive field plotted as a negative quantity if the loop is square (open symbols). The inset in panel (c) is an expanded view of the data for small Cr thicknesses.

many of the polar MOKE loops showed a gentle approach to saturation, the saturation field was taken to be the field at which the polar Kerr intensity reached 96% of its maximum value.[37] BLS measurements were made at various points along the wedge with a field of 5 kOe applied parallel to the Fe hard axis. This field value was chosen to be sufficiently large as to saturate the sample at all points along the wedge. The spin wave frequencies that were obtained are plotted in Fig. 1(a), while the polar MOKE and in-plane easy axis saturation fields are plotted in Fig. 1(b) and 1(c), respectively. Where the in-plane easy axis MOKE loop was found to be square we have plotted the coercive field as a negative field value in Fig. 1(c) and used an open rather than a solid symbol.

The in-plane easy axis saturation field immediately reveals the oscillatory nature of the coupling. Two regions of AFM coupling exist, in the first the Cr thickness varies between 4 and 15 Å, while the second begins at a Cr thickness of 20 Å and continues to the end of the Cr wedge where the Cr layer is 38 Å thick. For Cr thicknesses less than 4 Å and for Cr thicknesses between 16 and 20 Å, the easy axis loops are square, indicating that the sample is either FM coupled or

simply uncoupled. While the Cr gradient was determined to be 3.3 Å/mm from the thickness calibration, the point at which the Cr wedge begins is not known exactly beforehand. However, we are able to identify the beginning of the wedge as the point at which the coercivity of the easy axis loop decreases abruptly to about half its previous value, as shown in the inset in Fig. 1(c). We suggest that the inclusion of a partial Cr layer in the middle of a 40 Å Fe layer provides new sites for domain nucleation that reduce the coercive field. It is interesting to compare the easy axis loop saturation field scan with the polar MOKE saturation field scan. The first AFM region, with maximum coupling field at a Cr thickness of about 8 Å, is clearly visible in the polar MOKE scan but the second AFM region is less well defined. Both in-plane and polar MOKE loops are subject to optical effects so that the Kerr intensity may not vary exactly linearly with the magnetization component parallel to the applied field. Also the curvature of the loops depends upon the relative amounts of bilinear and biquadratic coupling present and so our method of determining the polar MOKE saturation field is subject to an error that may vary as we scan along the wedge. From Eq. (4) we saw that the polar MOKE saturation field does not in general have a linear dependence upon the coupling strength and therefore we do not expect an exact correspondence between the in-plane and polar MOKE saturation field scans. The polar MOKE does, however, give an excellent qualitative impression of the nature of the coupling. Particularly in the region where the Cr thickness varies from 0 to 4 Å we see a sharp reduction of the polar MOKE saturation field which we believe is due to strong ferromagnetic coupling of the two Fe layers. As a partial layer of Cr is introduced into the middle of the 40 Å Fe layer the saturation field decreases because of the additional perpendicular anisotropy associated with the Cr layer. The saturation field decreases until full Cr coverage is obtained. It is known that a monolayer of Cr orders antiferromagnetically with a neighboring Fe layer[15,40] so that at this point we expect to have two 20 Å Fe layers that are strongly FM coupled. As the Cr thickness increases further the FM coupling decreases and the polar MOKE saturation field increases. When the Cr thickness reaches a value of about 4 Å the coupling becomes antiferromagnetic and the saturation field increases further in a manner similar to the in-plane MOKE saturation field. For a Cr thickness of 16 Å the two Fe layers are essentially uncoupled, as is discussed below, and then the polar MOKE saturation field is seen to lie about half-way between the two extremal values observed for small Cr thicknesses.

Two spin wave modes are expected in the BLS experiment which correspond to an in-phase and out-of-phase precession of the magnetizations in the two Fe layers. These are referred to as the acoustic and optical spin wave modes, respectively. For the case that the sample is magnetically saturated, the acoustic mode is the more intense of the two modes but it is the optical spin wave mode frequency which is most sensitive to the interlayer coupling and indeed we see from Fig. 1(a) that it is the frequency of the optical mode that varies strongly as a function of Cr thickness. The optical mode was only sufficiently intense so as to be observable for Cr thicknesses between 11 and 30 Å. We see two modes in

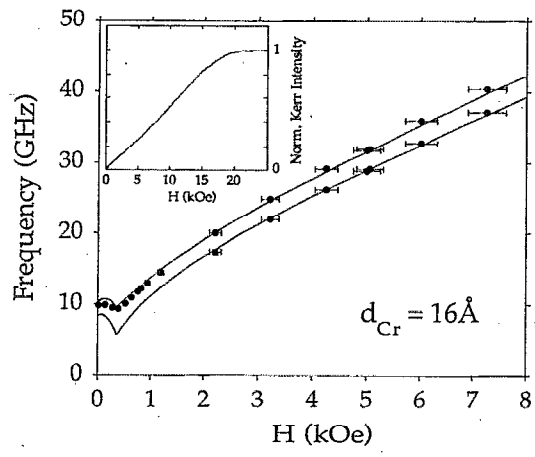

FIG. 2. BLS mode frequencies are plotted as a function of the applied field strength for the point on sample I at which the value of the Cr layer thickness is equal to 16 Å. The field was applied parallel to one of the Fe ⟨011⟩ hard axes. The curves have been fitted to the data. The inset shows the corresponding polar MOKE loop which exhibits two clear kinks at the points at which the two Fe layers saturate.

the region between the first and second AFM regions where the in-plane MOKE loops are square (Fig. 1) and here the mode with higher frequency is always the more intense. This means that the exchange coupling can only be very weakly FM and is insufficient to overcome the dipolar coupling which is weakly AFM. In fact, from a detailed calculation we have determined that the quantity $A_{12}+2B_{12}$ must lie in the range of 0.0–0.034 erg/cm^2. At the thin end of the wedge we see that there is a small jump in the acoustic mode frequency at a Cr thickness of about 2 Å, which corresponds roughly to the minimum in the polar MOKE saturation field. As the Cr thickness is decreased to zero we expect the acoustic mode to correspond to the surface mode of the 40 Å Fe layer, while the optical mode observed in the trilayer must evolve into the first volume mode of the 40 Å layer. This volume mode lies at a much higher frequency because of the large associated exchange energy. We therefore expect that in the 0–10 Å Cr region the optical mode frequency must change rapidly from a small value in the AFM region to a large value in the limit of zero Cr thickness and that the acoustic and optical modes must cross over at some intermediate point. The precise variation of the mode frequencies in this region is difficult to predict since it depends upon the Cr thickness dependence of both the interface anisotropy and interlayer coupling energies and these are strongly affected by the initial growth mode of the Cr. While we cannot conclude very much about the ultrathin Cr limit from the BLS data presented here, this does suggest how BLS might be useful when both acoustic and optical spin wave modes are observable.

In order to determine the values of the interface and cubic anisotropy fields for the two Fe layers for larger Cr thicknesses, we have made BLS measurements at a number of field values for the point on the wedge at which the Cr thickness has a value of 16 Å (Fig. 2). The interlayer exchange coupling field, which appears in Eqs. (2) and (5), changes sign at this point and so can be assumed to be negligible. Indeed the polar MOKE curve shown in the inset in

Fig. 2 shows a well defined kink which suggests that the interlayer exchange coupling is small. Any exchange coupling, either FM or AFM, would be expected to make the curve more rounded. At lower fields the curve has a small positive curvature ($\partial^2 M/\partial H^2 > 0$) which is due to the positive cubic anisotropy of the Fe and which may be exaggerated by a small quadratic dependence of the polar Kerr intensity upon the value of the magnetization component parallel to the polar axis. We have assumed that the two Fe layers are identical apart from their interface anisotropy constants. We assume the bulk Fe values of 1710 emu/cm^3 for the Fe layer magnetization and 2.09 for the g factor. The fit in Fig. 2 was obtained with the reduced calculation described in the previous section. From the best fit we deduce a value for the cubic anisotropy constant K_1 of 3.1×10^5 erg/cm^3 and values of 0.30 and 0.60 erg/cm^2 for the surface anisotropy constants of the two layers. These surface anisotropy constants are averaged over the two interfaces of each Fe layer and the larger value applies to the Fe layer with one Cr and one Ag interface while the smaller value applies to that with two Cr interfaces. The fact that these two constants are not equal means that the quantity H_a defined in Eq. (3) is different for the two layers and so Eq. (4) rather than Eq. (5) must be used in considering the polar MOKE saturation fields. Also we may infer values of 0.30 and 0.90 erg/cm^2 for the surface anisotropy constants of the Fe/Cr and Fe/Ag interfaces, the latter comparing well with previously reported values.[41] The value deduced for the cubic anisotropy constant is smaller than the bulk value of 4.5×10^5 erg/cm^3 but we note that other recent studies[42] have provided evidence that the magnetocrystalline volume anisotropy of an epitaxial ultrathin film may not obtain its bulk value until the film is some tens of angstroms thick.

We should at this point comment upon some of the underlying assumptions that have been made in the fitting procedure that we have just described. If the magnetizations of the two Fe layers were significantly different then this would greatly complicate the analysis; however, we have no reason to believe that this is the case. If, contrary to our assumption, the Fe layer magnetizations were equal but reduced from the bulk value then the deduced anisotropy and coupling parameters would need to be rescaled. This rescaling is, however, a simple procedure since the effective demagnetizing fields, $4\pi M - 4K_{s,i}/Md$, and the cubic anisotropy fields $2K_{1,i}/M$ of the two layers, and the coupling fields, A_{12}/M and B_{12}/M, should be unchanged by the assumption of a different magnetization value. For the 16 Å Cr point we neglected the effects of coupling although we knew only that the quantity $A_{12}+2B_{12}$ was approximately equal to zero. In fact in this case it can be shown that the individual values of A_{12} and B_{12} do not affect the calculation of the BLS frequencies so long as the static magnetizations of the two layers remain approximately collinear. This is certainly the case for the high-field BLS data which were used to obtain the values of the surface anisotropy constants. However, when a small field is applied parallel to the in-plane hard axis the magnetizations remain collinear only if, in addition to the magnetization, the cubic anisotropy constant K_1 is also the same for the two Fe layers. We have assumed that these two values of

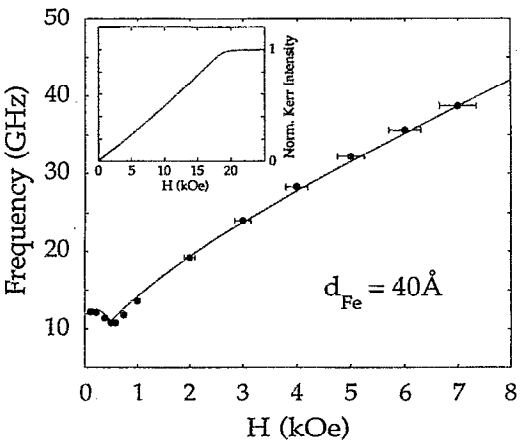

FIG. 3. The BLS mode frequency is plotted as a function of the applied field strength at the point just before the Cr wedge begins in sample I. The field was applied parallel to one of the Fe ⟨011⟩ hard axes and the curve is a fit to the data. The inset shows the corresponding polar MOKE loop.

K_1 are identical since the Fe layers are of identical thickness and because we have no evidence to the contrary. If this assumption were in fact incorrect then the values of A_{12} and B_{12} estimated below for other points on the sample would be modified although this modification is only expected to be significant for the case of weak coupling when the anisotropy and coupling fields are of similar magnitude.

A BLS field scan was also performed for a point just before the beginning of the Cr wedge. The measured frequencies and the corresponding polar MOKE curve are shown in Fig. 3. Only one spin wave mode is observed and the polar MOKE curve shows a smooth approach to saturation, with a little positive curvature induced by the cubic anisotropy, as expected for a single 40 Å Fe layer. The best fit value for the cubic anisotropy constant is now 4.3×10^5 erg/cm^3, close to the bulk value, while the best fit value for the surface anisotropy constant is 0.72 erg/cm^2. This latter value compares with the value of 0.60 erg/cm^2 obtained previously for a 20 Å layer with similar interfaces and the agreement can be seen to be quite good when we bear in mind that we have not included other possible contributions to the perpendicular anisotropy such as magnetoelastic anisotropy. The values of the anisotropy constants determined for the various Fe layers in this study are shown in Table I.

In the first AFM coupling peak it was possible to fit the easy axis in-plane MOKE loops by assuming that the system occupies the minimum energy state. The parameter values obtained from the BLS fit to the 16 Å Cr point were assumed and the coupling parameters A_{12} and B_{12} were varied to

TABLE I. The parameter values determined by BLS for the Fe layers in sample I are shown. In addition, values of 1710 emu/cm^3 and 2.09 were assumed for the magnetization and g factor of the Fe layers.

Layer	K_1 ($\times10^5$ erg/cm^3)	K_s (erg/cm^2)
Cr/Fe(20 Å)/Ag	3.1	0.60
Cr/Fe(20 Å)/Cr	3.1	0.30
Cr/Fe(40 Å)/Ag	4.3	0.72

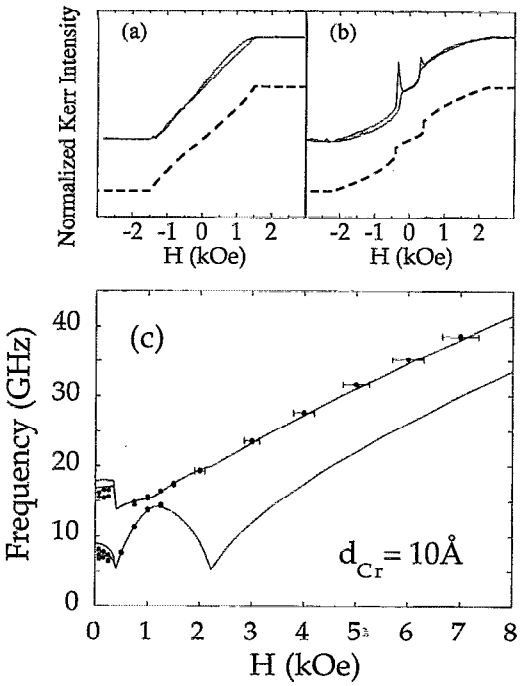

FIG. 4. The in-plane easy and hard axis MOKE loops and BLS mode frequencies are shown in panels (a), (b), and (c), respectively, for the point on sample I at which the Cr layer thickness has a value of 10 Å. The field was applied parallel to one of the Fe ⟨011⟩ hard axes in (c) and the curves are fits to the data. The best-fit parameters from (c) were used to generate the dashed curves in (a) and (b).

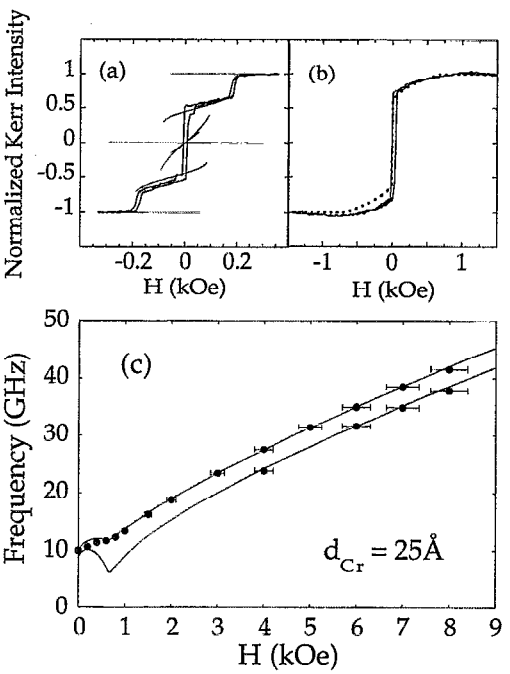

FIG. 5. The in-plane easy and hard axis MOKE loops and BLS mode frequencies are shown in panels (a), (b), and (c), respectively, for the point on sample I at which the Cr layer thickness has a value of 25 Å. The field was applied parallel to one of the Fe ⟨011⟩ hard axes in (c) and the curves are fits to the data. The best-fit parameters from (c) were used to generate the theory curves in (a) and (b). In the case of (a), branches representing all the local energy minima have been plotted.

obtain the best fit. BLS field scans have been used previously to investigate interlayer coupling[14,43–45] and we have performed a BLS field scan at the point at which the Cr thickness has a value of 10 Å for comparison with the MOKE data. The measured frequencies and the in-plane hard and easy MOKE loops are shown in Fig. 4. For the BLS scan we see that for large field values only one mode is observed but as the field is reduced from the saturation value the magnetizations in the two layers cant apart and two modes are again observed. At a smaller field of approximately 0.4 kOe the magnetizations jump to an almost antiparallel alignment and then the Stokes and anti-Stokes modes are observed to have slightly different frequencies. This is due to the nonreciprocal nature of the spin wave modes which leads to different dipolar interactions for spin waves travelling in opposite directions as has been previously noted.[1] It has been reported[45] that the mode frequencies in this region are very sensitive to the exact values of the layer thicknesses and so we have not included these points in our fit. Consequently the agreement between the theory curve and the data is good except in the low-field region. We have recalculated all the theory curves in this article using the full BLS theory described previously. The difference between the frequencies obtained from the full and reduced theories is found to be small except in the vicinity of the saturation field. At this point differences of up to 3 GHz occur for the low-frequency-mode calculation. We have not been able to observe the low-frequency mode close to the saturation field in our measurements and we believe that the difference between the two theories is acceptably small for the data points that we have used in our fits. Values of -0.14 and -0.010 erg/cm^2 were obtained for A_{12} and B_{12}, respectively, from the fit to the BLS field scan shown in Fig. 4(c). These values were used to calculate the expected MOKE loops and these are plotted with the experimental data in Fig. 4(a) and (b). The saturation and switching fields of both the easy and hard axis loops are well reproduced by the theoretical curves although the curvature of the experimental loops is found to be slightly different. Indeed, the fit of the easy axis MOKE loop yielded values of -0.11 and -0.022 erg/cm^2 for A_{12} and B_{12}, respectively. A simulation using these parameters produced a very poor fit to the BLS data. This illustrates how the coupling parameters determined by MOKE may depend upon the curvature of the MOKE loops which is not necessarily the same as that of the true magnetization curve. We should of course bear in mind that contrary to our assumption the two Fe layers may have slightly different thicknesses, magnetizations, or cubic anisotropy constants and that this may also influence the curvature of the observed loops. The layer magnetizations might also possess some spatial nonuniformity which has not been accounted for in the modeling of either the BLS or the MOKE data.

In the second AFM coupling region it became difficult to reliably determine the values of A_{12} and B_{12} from the in-plane MOKE loops. The easy and hard axis loops for the point at which the Cr thickness has a value of 25 Å are plotted in Figs. 5(a) and 5(b), respectively. At remenance the

sample is observed to occupy a state in which the layer magnetizations lie 90° apart along different cubic easy axis directions, suggesting that the biquadratic coupling is significant. For the hard axis loop the applied field causes the magnetizations to rotate gradually toward the field direction. We find that if the quantity $A_{12}+2B_{12}$ is fixed so as to keep the saturation field constant, the effect of varying the ratio of B_{12} to A_{12} is to only slightly modify the curvature of the loop. For the easy axis loop, once the remenant 90° state is established, the saturation field is the only feature that we might attempt to fit. However, if the coupling field is small compared to the cubic anisotropy field, as in this case, this is unfortunately not possible. A coherent rotation calculation [Eq. (3)] would predict that the loop should be square while the assumption that the system must reside in the minimum energy state may be flawed since the reversal process is not known. In fact, for a pair of candidate values of A_{12} and B_{12}, we may only establish which states exist at a given field value and then check that the experimental data corresponds to one of these states. The BLS field scan obtained at this point is shown in Fig. 5(c). The best fit to the data yields values of -0.0099 and -0.0079 erg/cm^2 for A_{12} and B_{12}, respectively, which implies a value of 0.80 for the ratio of B_{12} to A_{12}. In fact we find that a 90° state with one of the layer magnetizations parallel to the field direction only exists at the observed easy axis saturation field if this ratio has a value less than about 0.9. It may seem odd that this is an upper rather than a lower limit, but there is a simple physical interpretation. When the coupling field is small and of the same order as the cubic anisotropy field then a close to 90° state exists at remenance. The biquadratic coupling exerts only a small torque between the two magnetizations in this case. As the applied field is increased it is the bilinear coupling that provides the torque to counteract that due to the applied field and so it is the bilinear coupling that is effective in stabilizing the 90° state at higher applied field values. The values of A_{12} and B_{12} determined by BLS are therefore fully consistent with the observed MOKE loops. The theory curves in Fig. 5(a) and 5(b) assume the BLS best fit parameter values. The hard axis theory curve was calculated assuming that the system resides in a local energy minimum until that minimum becomes unstable. For the easy axis we have shown the magnetization component associated with each local energy minimum to demonstrate that the observed loop is feasible even if we do not know exactly how the system moves between the different local minima. The agreement between theory and experiment for the hard axis loop is reasonable given that the experimental loop is asymmetric and does not exhibit a clear saturation field. Again the presence of optical effects means that the experimental loop may not be a true magnetization curve. A BLS field scan was also performed for the point at which the Cr thickness is equal to 30 Å. Here the total coupling field is even smaller and it is consequently even more difficult to separate the values of A_{12} and B_{12}. The best fit to the BLS scan yielded values of -0.0080 and -0.0045 erg/cm^2 for A_{12} and B_{12}, respectively, which implies a value of 0.57 for the ratio of B_{12} to A_{12}. Unfortunately the fit is not very sensitive to this ratio and the MOKE loops did not permit us to put narrow bounds on its value so the best fit value of the ratio of A_{12} to B_{12} may be subject to a large error.

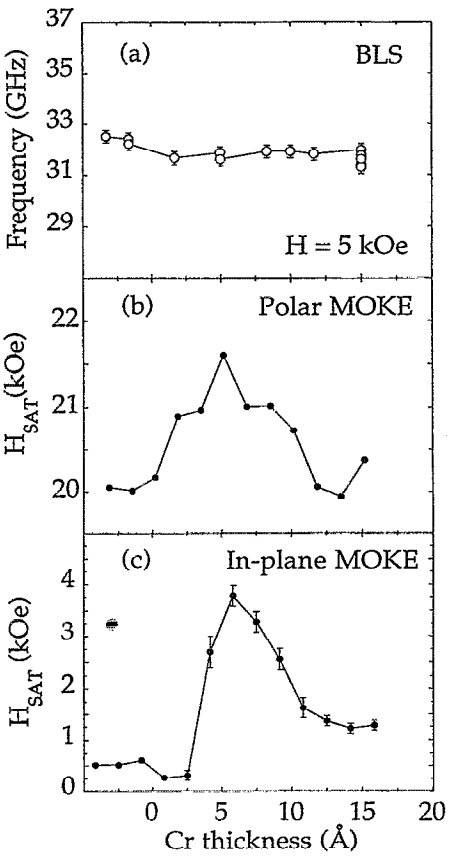

FIG. 6. The following quantities are plotted as a function of Cr thickness for sample II: (a) the BLS acoustic mode frequency; (b) the polar MOKE loop saturation field; (c) the in-plane hard axis MOKE saturation field.

A second sample (sample II) was studied which was identical to sample I except that the Cr layer thickness was intended to be in the range of 0–20 Å. The in-plane and polar MOKE saturation fields and the BLS frequencies for various points on the wedge are shown in Fig. 6. Unfortunately this sample has since deteriorated and only the original course scale data is available; however, this is still useful in investigating the repeatability of the observed coupling strengths. For the in-plane MOKE scan in Fig. 6(c) we have plotted the hard axis saturation field as opposed to the easy axis saturation field that was plotted in Fig. 1(c). We notice here that a drop in the hard axis saturation field has been used to identify the beginning of the Cr wedge. The saturation field of the 40 Å Fe layer is approximately 0.5 kOe while this value drops to about 0.3 kOe when the Cr layer is introduced, just as for the first sample. The peak hard axis saturation field of 3.75 kOe in Fig. 6(c) corresponds to an easy axis saturation field of about 3 kOe which is in good agreement with that observed in Fig. 1(c) and hence suggests that the total coupling strength in the two samples is similar. The polar MOKE saturation fields in Fig. 6(b) are somewhat larger than those in Fig. 1(b) and only one mode was observed in the BLS measurements even at small applied fields.

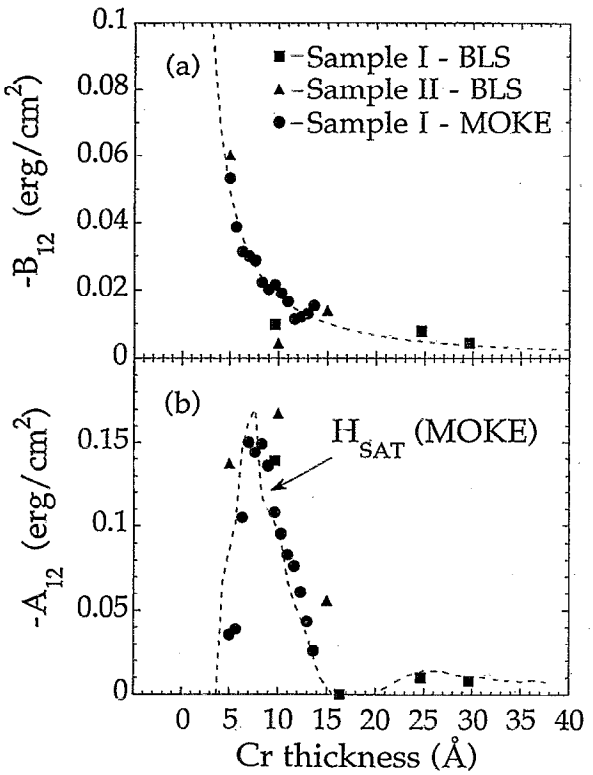

FIG. 7. The values of the coupling constants B_{12} and A_{12} for samples I and II are plotted as a function of Cr thickness in panels (a) and (b), respectively. The meaning of the various symbols is indicated in panel (a). The curve in panel (a) has been fitted to the data while the curve in panel (b) is a scaled version of the curve in Fig. 1(c) that serves only to guide the eye.

Despite this it was found to be possible to fit BLS field scans with the same parameters for the Fe layers as for the first sample. We note that the acoustic mode is in fact sensitive to the values of the coupling parameters in the low-field regime where canting of the Fe layer magnetizations occurs. The values of A_{12} and B_{12} deduced from BLS and MOKE measurements for both samples I and II are displayed in Fig. 7.

V. DISCUSSION

We begin by comparing our values for the coupling strengths in the Fe/Cr/Fe system with those obtained by other researchers. From the separation of the maxima of the first and second peaks in the easy axis saturation field in Fig. 1(c) we obtain a value of about 18 Å for the long period of oscillation in the coupling strength. Taking the lattice parameter of Cr to be 2.87 Å we see that this agrees well with the value of 12±1 monolayers (17.2±1.4 Å) deduced for samples grown on Fe whisker substrates.[13] The position of our first coupling maximum at 8 Å of Cr lies close to the observed position of the first short period AFM coupling maximum at 5 monolayers (7.2 Å) of Cr.[14] We observe the coupling strength to be offset in the AFM direction as has been observed by other researchers.[14,29,46] After taking into account the different definitions of the coupling energy used by different authors we note that in studies for which short period coupling oscillations are observed,[14,29] and also for other samples grown on Ag/GaAs(100) for which short period oscillations were not observed,[46] the maximum coupling strength was found to be at least three times as large as that shown in Fig. 7. This cannot be explained by the fact that thicker Fe layers were used by other researchers since the coupling strength is actually expected to increase with decreasing Fe layer thickness.[47] We therefore believe that it is likely that some structural imperfection is responsible for attenuating the total (bilinear plus biquadratic) coupling strength in our samples.

From Fig. 7 we see that the biquadratic coupling constant B_{12} is largest for small Cr thicknesses. Dominant biquadratic coupling at small Cr thicknesses has also been observed for samples grown on Fe whisker substrates[13] while the form of the curves for A_{12} and B_{12} in the first AFM coupling region are similar to those presented in Ref. 17. We have explained that it is difficult to accurately determine the values of A_{12} and B_{12} in the second AFM coupling region because the coupling field is of similar size to the cubic anisotropy field. However, our best fits indicate that the ratio of B_{12} to A_{12} in the center of this region is of the order of 0.8 which is larger than the value of 0.26 obtained previously[6] for samples grown on Ag/GaAs(100) substrates. In the latter case it was found that the biquadratic coupling became dominant at somewhat larger Cr thicknesses,[46] in the third AFM coupling region. By fitting a straight line to a log plot of the data in Fig. 7(a) we find that B_{12} varies approximately as $d_{\mathrm{Cr}}^{-1.4}$ over the full range of Cr thicknesses studied. The thickness dependence of B_{12} can in principle be predicted from the various extrinsic models of biquadratic coupling but in order to do this one must determine how the relevant structural imperfection varies with the thickness of the Cr spacer layer. If we assume that the interfacial roughness, the distribution of loose spins, and the density of pinholes are all independent of the Cr thickness then both the loose spins mechanism and the mechanisms depending upon interfacial roughness predict that the biquadratic coupling should decrease monotonically with Cr thickness as we indeed observe. The power-law behavior of B_{12} and the reduced values of A_{12} observed in our data may therefore provide a quantitative test of extrinsic coupling theories.

In conclusion, MOKE and BLS measurements have been combined in order to determine the dependence of the interlayer coupling constants upon the Cr thickness in Fe/Cr/Fe trilayer samples. While short period coupling oscillations have not been observed we find that the phase and period of the long period oscillations agree well with those reported by other researchers. The coupling is however weaker in our samples which we attribute to the presence of structural imperfections. We observe a large value for the ratio of the biquadratic to bilinear coupling strengths at the beginning of the first AFM coupling region and also in the second AFM coupling region, the thickness dependence of the biquadratic coupling constant being well described by a $d_{\mathrm{Cr}}^{-1.4}$ power law. In view of the suspected structural imperfections in our samples we believe that this data may be useful in testing the extrinsic models that have been proposed for the biquadratic coupling mechanism. We have also shown that the coercivity of the easy axis MOKE loop is sensitive to submonolayer

coverages of Cr and demonstrated that polar MOKE and BLS may be particularly useful in investigating the ultrathin Cr regime where the coupling is strongly FM in nature and the magnetic structure of the Cr is strongly influenced by reduced dimensionality and topological effects.

ACKNOWLEDGMENTS

The financial support of the EPSRC, the Toshiba Corporation, the Alliance Programme of the British Council, and the Newton Trust, Cambridge, for this work is gratefully acknowledged. M. G. would like to thank the EC for a bursary (Contract No. BREU-900293). S. J. G. would like to thank the DRA, U. K., for support.

[1] P. Grünberg, R. Schreiber, Y. Pang, M. D. Brodsky, and H. Sowers, Phys. Rev. Lett. **57**, 2442 (1986).
[2] M. N. Baibich, J. M. Broto, A. Fert, F. Nguyen Van Dau, F. Petroff, P. Etienne, G. Creuzet, A. Friederich, and J. Chazelas, Phys. Rev. Lett. **61**, 2472 (1988).
[3] *Ultrathin Magnetic Structures II*, edited by J. A. C. Bland and B. Heinrich (Springer, Berlin, 1994).
[4] J. J. Krebs, P. Lubitz, A. Chaiken, and G. A. Prinz, Phys. Rev. Lett. **63**, 1645 (1989).
[5] S. S. P. Parkin, N. More, and K. P. Roche, Phys. Rev. Lett. **64**, 2304 (1990).
[6] M. Rührig, R. Schäfer, A. Hubert, R. Mosler, J. A. Wolf, S. Demokritov, and P. Grünberg, Phys. Status Solidi A **125**, 635 (1991).
[7] E. Fawcett, Rev. Mod. Phys. **60**, 209 (1988).
[8] S. T. Purcell, W. Folkerts, M. T. Johnson, N. W. E. McGee, K. Jager, J. van de Stegge, W. B. Zeper, and W. Hoving, Phys. Rev. Lett. **67**, 903 (1991).
[9] J. Unguris, R. J. Celotta, and D. T. Pierce, Phys. Rev. Lett. **67**, 140 (1991).
[10] J. Unguris, R. J. Celotta, and D. T. Pierce, Phys. Rev. Lett. **69**, 1125 (1992).
[11] P. Bruno, J. Magn. Magn. Mater. **121**, 248 (1993); Phys. Rev. B **52**, 411 (1995).
[12] E. E. Fullerton, M. J. Conover, J. E. Mattson, C. H. Sowers, and S. D. Bader, Phys. Rev. B **48**, 15 755 (1993).
[13] D. T. Pierce, J. A. Stroscio, J. Unguris, and R. J. Celotta, Phys. Rev. B **49**, 14 564 (1994).
[14] B. Heinrich, M. From, J. F. Cochran, L. X. Liao, Z. Celinski, C. M. Schneider, and K. Myrtle, Mater. Res. Soc. Symp. Proc. **313**, 119 (1993).
[15] C. Turtur and G. Bayreuther, Phys. Rev. Lett. **72**, 1557 (1994).
[16] A. Vega, L. C. Balbas, A. Chouairi, C. Demangeat, and H. Dreyssé, Phys. Rev. B **49**, 12 797 (1994).
[17] U. Köbler, K. Wagner, R. Wiechers, A. Fuss, and W. Zinn, J. Magn. Magn. Mater. **103**, 236 (1992).
[18] R. P. Erickson, K. B. Hathaway, and J. R. Cullen, Phys. Rev. B **47**, 2626 (1993).
[19] J. Barnas and P. Grünberg, J. Magn. Magn. Mater. **121**, 326 (1993).
[20] J. Barnas, J. Magn. Magn. Mater. **123**, L21 (1993).
[21] D. M. Edwards, J. M. Ward, and J. Mathon, J. Magn. Magn. Mater. **126**, 380 (1993).
[22] J. C. Slonczewski, J. Magn. Magn. Mater. **126**, 374 (1993).
[23] J. C. Slonczewski, Phys. Rev. Lett. **67**, 3172 (1991).
[24] S. Demokritov, E. Tsymbal, P. Grünberg, W. Zinn, and I. K. Schuller, Phys. Rev. B **49**, 720 (1994).
[25] J. C. Slonczewski, J. Appl. Phys. **73**, 5957 (1993).
[26] J.-F. Bobo, M. Piecuch, and E. Snoeck, J. Magn. Magn. Mater. **126**, 440 (1993).
[27] D. B. Fulghum and R. E. Camley (unpublished).
[28] M. From, L. X. Liao, J. F. Cochran, and B. Heinrich, J. Appl. Phys. **75**, 6181 (1994).
[29] P. Grünberg, A. Fuss, Q. Leng, R. Schreiber, and J. A. Wolf, in *Magnetism and Structure in Systems of Reduced Dimension*, NATO ASI series (1992).
[30] J. R. Waldrop and R. W. Grant, Appl. Phys. Lett. **34**, 630 (1979).
[31] J. J. Krebs, B. T. Jonker, and G. A. Prinz, J. Appl. Phys. **61**, 2596 (1987).
[32] M. Gester, Ph.D. thesis, University of Cambridge, 1994.
[33] P. Etienne, J. Massies, F. Nguyen Van Dau, A. Barthélémy, and A. Fert, Appl. Phys. Lett. **55**, 2239 (1989).
[34] J. Yuan, E. Gu, M. Gester, J. A. C. Bland, and L. M. Brown, J. Appl. Phys. **75**, 6501 (1994).
[35] C. Daboo, J. A. C. Bland, R. J. Hicken, A. J. R. Ives, M. J. Baird, and M. J. Walker, Phys. Rev. B **47**, 11 852 (1993).
[36] B. Dieny, J. P. Gavigan, and J. P. Rebouillat, J. Phys. Condens. Matter **2**, 159 (1990); B. Dieny and J. P. Gavigan, *ibid.* **2**, 187 (1990).
[37] A. J. R. Ives, R. J. Hicken, J. A. C. Bland, C. Daboo, M. Gester, and S. J. Gray, J. Appl. Phys. **75**, 6458 (1994).
[38] R. J. Hicken, D. E. P. Eley, A. J. R. Ives, C. Daboo, J. A. C. Bland, J. R. Childress, and A. Schuhl, Phys. Rev. B **50**, 6143 (1994).
[39] J. F. Cochran, J. Rudd, W. B. Muir, B. Heinrich, and Z. Celinski, Phys. Rev. B **42**, 508 (1990).
[40] R. Jungblut, C. Roth, F. U. Hillebrecht, and E. Kisker, J. Appl. Phys. **70**, 5923 (1991); T. G. Walker, A. W. Pang, and H. Hopster, Phys. Rev. Lett. **69**, 1121 (1992).
[41] B. Heinrich and J. F. Cochran, Adv. Phys. **42**, 523 (1993).
[42] J. Fassbender, Ch. Mathieu, B. Hillebrands, G. Güntherodt, R. Jungblut, and M. T. Johnson, J. Appl. Phys. **76**, 6100 (1994).
[43] P. Kabos, C. E. Patton, M. O. Dima, D. B. Church, R. L. Stamps, and R. E. Camley, J. Appl. Phys. **75**, 3553 (1994).
[44] M. Macciò, M. G. Pini, P. Politi, and A. Rettori, Phys. Rev. B **49**, 3283 (1994).
[45] R. L. Stamps, Phys. Rev. B **49**, 339 (1994).
[46] S. Demokritov, J. A. Wolf, and P. Grünberg, Europhys. Lett. **15**, 881 (1991).
[47] S. N. Okuno and K. Inomata, Phys. Rev. Lett. **72**, 1553 (1994).